Spatial modeling of concrete strength based on data

Sebastian Geyer[a,*], Iason Papaioannou[a], Daniel Straub[a]

[a]*Engineering Risk Analysis Group, Technische Universität München, Arcisstr. 21, 80290 München, Germany*

Abstract

Structural verification of concrete structures relies on an underlying probabilistic model of the concrete strength. This concrete strength exhibits a spatial variability, which is of particular relevance in existing concrete structures, for which the strength is assessed based on samples. To accurately account for the spatial variability of the concrete material, a random field modeling approach can be adopted, which includes a spatial correlation function. Unfortunately, the available literature on spatial variability of concrete strength is not sufficient to make an educated choice of this correlation function. In this paper, we propose a hierarchical Bayesian random field model, that enables learning the parameters of a selected correlation function with in-situ spatially distributed measurements of the concrete strength. We propose a correlation function that accounts for the composite nature of the material through distinguishing micro-scale and meso-scale variability. The predictive spatial distribution of the proposed random field model given the spatial data is then obtained through an analytical random field update, resulting in a non-homogeneous random field model with log-Student's t-marginal distribution. The proposed approach provides an effective means to employ in-situ measurements for updating verification predictions of concrete structures. We apply our approach to two case studies on chamber walls of ship locks, where measurements of the concrete strength are available from core samples.

Keywords: Spatial variability, Concrete strength, Bayesian analysis, Hierarchical model, Concrete correlation model, Structural verification

*Corresponding author
Email address:* `s.geyer@tum.de` (Sebastian Geyer)

1. Introduction

Structural analysis and verification requires the specification of material strength parameters. These parameters are subject to uncertainty, which needs to be accounted for in the analysis. In many instances, a conservative characteristic value of the strength parameter is employed to account for this uncertainty [1, 2, 3]. For the design of new structures, such values are given through the material classification, such as steel grade or concrete strength class [4, 5]. In contrast, the assessment of existing concrete structures typically relies on samples taken from the structure to estimate the characteristic value of the concrete strength [6, 7]. This is done via standardized procedures, which are based on assumptions on the underlying probability distribution model for the concrete strength [7, 3, 8]. These approaches do not account for a potential correlation of the measurements as they assume the samples to be drawn independently from a certain population (the structure of interest) [9, 10]. Neglecting such a correlation leads to approximate results. The extent of the approximation error is case-specific; it is larger in older concretes with higher variability in the concrete strength.

We focus on the assessment of existing structures where concrete strength exhibits higher variability and is commonly assessed based on samples from the actual structure. The corresponding measurement values and their locations provide the basis for a spatial analysis [11]. For these applications, we suggest to model concrete strength as a random field, whereby a random variable is assigned to each position in the structure. The dependence among the random variables at all locations is described by a spatial correlation function [12].

An approach to model the concrete strength as a random field has been proposed in the context of the JCSS probabilistic model code [13]. However, this model is not appropriately reflecting the interplay between inter- and intra-site variability. Generally, the existing literature on random field models for concrete strength is rather sparse and has mostly found application in initial studies on structural reliability or response analysis [14, 15] or in investigations of its microstructure [e.g., 16, 17]. An extensive study has been carried out in [18] to investigate the variability of concrete strength within a structure in the context of seismic design of existing structures. Recently, an approach to model concrete strength on multiple hierarchical levels with focus on the hierarchy originating from the construction process has been proposed, where it is suggested to model the variability within a structural component with a random field [19]. In [20], the authors apply a hierarchical random field model to obtain location-specific characteristic values of the concrete strength. Therein, an assumption on the prior correlation function of the concrete strength is made relying on the limited available literature.

The modeling approach in this paper uses Bayesian methods to learn the distribution of the concrete strength through combining measurements with available prior information [21]. It employs the hierarchical modeling approach also used in [20], where not only the spatial variability but also the uncertainty of the

distribution parameters is explicitly modeled and learned from the data [22, 9]. Hence, our model accounts for both the intra- and inter-site variability, the latter reflected by the uncertain distribution parameters. To take into account the nature of concrete as a composite material, a novel spatial correlation model is developed, whose parameters can also be included in the Bayesian learning, hence, circumventing the need for an ad-hoc choice of the spatial correlation function. The resulting predictive random field has log-Student's t-marginal distribution and can be expressed as function of a Gaussian random field through a simple transformation [22]. The derived distribution model can be used in further uncertainty propagation and reliability analyses as well as to compute the spatial distribution of the characteristic value of the concrete strength to be used in structural verifications.

The remainder of the paper is structured as follows: Section 2 briefly reviews the definition of the concrete compressive strength and its characteristic value, before introducing a hierarchical spatial model and describing the Bayesian learning of its parameters. Section 3 applies the methodology to two ship lock data sets, followed by a discussion and interpretation of the obtained results. The analysis of these data sets provides empirical evidence on concrete strength correlation in practice, but also highlights the challenges associated with the use of the spatial model in practice. Section 4 gives a brief summary of the results and conclusions. Some additional information on the log-Student's t-distribution are collected in the Appendix.

2. Statistical modeling of concrete compressive strength

The strength of concrete depends on different factors, e.g., the water-cement ratio, the size and shape of the included aggregate, used admixtures or the quality of workmanship in the production process [e.g., 23, 13, 24]. The dominating strength parameter of concrete is its compressive strength f_c, which is the focus of this paper. The parameter f_c is used to classify concrete into different concrete classes (grades). In the following, we propose a spatial probabilistic model for f_c, and in Section 2.4 we show how the distribution can be learned with measurement data.

2.1. Compressive strength of concrete

Concrete is a composite material made of water, cement, aggregate and potential admixtures. After the hardening process, concrete can be divided into two phases, cement matrix and aggregate. Due to the two-phase nature of the concrete material, defining f_c as a point-in-space continuous property is not meaningful. Instead, f_c is defined as the compressive strength of a volume of finite size [25]. f_c depends not only on the compressive strengths of cement matrix and aggregate alone, but also on the quality of the connection between the two phases, which is determined by factors such as the surface of the aggregate and the type of cement [26]. Furthermore, f_c depends on other factors that are not directly related to the material itself, such as the direction of stress or the strain constraint due to size effects [27, 26, 1].

3

Due to the reasons above, the compressive strength of concrete is assessed in terms of the breaking load on reference specimens that have the shape of a cylinder ($f_{c,\mathrm{cyl}}$) or a cube ($f_{c,\mathrm{cube}}$) [25, 4, 13, 9]. Nowadays, typical cylinder specimen have a height-diameter ratio of 2 (e.g., a height of 300 mm and a diameter of 150 mm) and cube specimen have an edge length of 150 mm [25]. Cubical specimen are mostly used for verifications during the construction process as part of the quality control process. In contrast, cylindrical specimen are typically used in verifications of existing structures based on core samples taken from the structure. Classification of concrete into different strength classes is done with respect to requirements for $f_{c,\mathrm{cyl}}$ and $f_{c,\mathrm{cube}}$ [4]. The structural verification format of the Eurocode series is based on $f_{c,\mathrm{cyl}}$ as the critical parameter for all verifications regarding compression [4]. This paper focuses on modeling the concrete strength of existing structures and thus we employ $f_{c,\mathrm{cyl}}$ to denote the in-situ concrete strength.

Depending on the application at hand, the structural resistance R can differ from $f_{c,\mathrm{cyl}}$, e.g., when accounting for size effects [e.g., 27, 1] or when $f_{c,\mathrm{cyl}}$ is used to infer other concrete parameters. In these cases, R is a function of $f_{c,\mathrm{cyl}}$, which will introduce additional uncertainty into the model. However, the focus of this paper lies on the probabilistic model of $f_{c,\mathrm{cyl}}$ and such uncertainty is not further investigated.

To improve readability, f_c denotes the compressive strength of a cylindrical core sample for the remainder of this paper.

2.2. Characteristic values of the concrete strength

Standardized verification formats rely on characteristic values $f_{c,\mathrm{k}}$ of the concrete strength. Characteristic values are generally defined as $p-$quantile values of an underlying probabilistic model, where p depends on the property and the type of analysis. The $5\%-$quantile value is typically chosen as characteristic value for the concrete compressive strength [3]:

$$f_{c,\mathrm{k}} = F_{f_c}^{-1}(p) = F_{f_c}^{-1}(0.05), \tag{1}$$

where $F_{f_c}^{-1}(\cdot)$ is the inverse cumulative distribution function (CDF) of the concrete compressive strength.

When strength data from in-situ concrete samples are available, they can be used to estimate the characteristic value $f_{c,\mathrm{k}}$. Different approaches have been developed and established in the engineering community to estimate $f_{c,\mathrm{k}}$ from data of in-situ concrete samples. The most common ones are based on sample moment estimates, i.e., the mean and variance of the samples, which are further used to obtain the characteristic value based on tabulated values [3, 7, 8]. While the approach in [8] is based on a frequentist perspective [10], the method in [3] and [7] relies on the Bayesian approach [9, 14, 22].

These approaches only require the number of measurements n_m and the measurement values and do not account for the spatial locations of the measurements. Moreover, they do not differentiate between the concrete strength of a standardized cylinder and the in-situ structural resistance. However, some prerequisites have to be fulfilled for their application: the measurements must be statistically independent, they have to

4

be taken randomly in space and the sample size needs to be representative for the quantity of interest [9, 10]. While the last condition is assumed to be fulfilled by requiring a minimum number of samples for a given structure (depending on the size of the structure) [7], little attention is paid to the other two conditions in practice and these conditions are commonly violated. For example, in many instances multiple samples are taken from the same drilling core and sample locations are selected based on the perceived criticality or importance of the material or location. Local clustering of data in limited areas of the structure can lead to erroneous estimates of the variability of the quantity of interest and, hence, an erroneous estimate of its characteristic value. In order to obtain an accurate estimate, it is important to explicitly account for the locations of the samples. To explicitly consider these locations, the spatial variability of the concrete material should be modeled by a random field model.

2.3. Hierarchical random field model

Material parameters that vary randomly in space, such as the strength of concrete f_c, can be modeled by random fields. A random field (RF) represents a random variable at every point $\boldsymbol{z}$ in the spatial domain Ω [12]. In practice, the probabilistic description of the RF is parameterized in a way that enables its definition through a finite set of parameters $\boldsymbol{\Theta}$, the parameters of the marginal RF distribution, and a spatial correlation function $\rho(\boldsymbol{z}, \boldsymbol{z}')$. In hierarchical random field models, the parameters in $\boldsymbol{\Theta}$ are modeled by random variables described by a probability density function (PDF) $f(\boldsymbol{\theta})$. Such a modeling approach enables distinguishing two different types of uncertainty: (i) the uncertainty associated with the parameters of the spatial distribution of the material property, and (ii) the spatial variability of the property for fixed parameters. Uncertainty (i) is related to the inter-structure variability, i.e., the variability of the material property when comparing different structures, whereas uncertainty (ii) represents the intra-structure variability, i.e., the variability of the property when comparing different locations within a specific structure. Examples of hierarchical random field models in the context of probabilistic material modeling can be found in [13, 9, 28]. In the following, we describe the two types of uncertainty in detail and set up a hierarchical RF model for f_c.

2.3.1. Intra-structure variability

The intra-structure spatial variability is modeled by a random field, which is a collection of random variables indexed by a continuous spatial coordinate $\boldsymbol{z} \in \Omega$ [12]. To completely define the RF $f_c(\boldsymbol{z})$, one needs to specify the joint distribution of the random variables corresponding to any selection of points in Ω. If this joint distribution is the multivariate Gaussian distribution for any collection of points, the corresponding RF is a Gaussian RF [29]. The use of a Gaussian RF is beneficial in practice due to its simple definition and the numerous computational advantages of the Gaussian distribution, which facilitate the numerical treatment of RFs, i.e., their representation in terms of a finite number of RVs [30, 31]. An RF is

said to be homogeneous, if the marginal distribution is space-invariant and the joint distribution is invariant to a shift in $\boldsymbol{z}$.

If the quantity of interest is non-Gaussian, it is a common practice to define the corresponding RF as function of a zero-mean and unit-variance Gaussian RF $U(\boldsymbol{z})$ to simplify its application in practice. This type of non-Gaussian RF is termed translation RF and can be defined through the following marginal transformation [32, 33]:

$$X(\boldsymbol{z}) = F_{X(\boldsymbol{z})|\boldsymbol{\theta}}^{-1}(\Phi(U(\boldsymbol{z}))), \tag{2}$$

where $F_{X(\boldsymbol{z})|\boldsymbol{\theta}}^{-1}(\cdot)$ is the inverse CDF of $X(\boldsymbol{z})$ conditional on the realization $\boldsymbol{\theta}$ of $\boldsymbol{\Theta}$ and $\Phi(\cdot)$ is the CDF of the standard normal distribution.

The assumption that f_c follows a normal or lognormal distribution has been accepted and applied for many years [e.g., 34, 35, 2]. The lognormal distribution is more appropriate in cases of low concrete strengths or/and large variability of the concrete strength, since it is only defined for non-negative values and, thus, cannot result in a negative characteristic value. We limit ourselves to the lognormal model, for which the transformation of Equation (2) in the case of a homogeneous RF is

$$f_c(\boldsymbol{z}) = \exp\left(\mu_{f_{c,\ln}} + \lambda_{f_{c,\ln}}^{-\frac{1}{2}} U(\boldsymbol{z})\right). \tag{3}$$

The parameters $\boldsymbol{\Theta} = [\mu_{f_{c,\ln}}, \lambda_{f_{c,\ln}}]$ are the mean value $\mu_{f_{c,\ln}}$ and precision $\lambda_{f_{c,\ln}}$ of $\ln(f_c)$, where $\lambda_{f_{c,\ln}}$ is the inverse of the variance. Using Equation (3), the spatial variability of $f_c(\boldsymbol{z})$ is implicitly modeled through the spatial variability of the underlying RF $U(\boldsymbol{z})$ and, thus, $f_c(\boldsymbol{z})$ is fully defined by the parameters of its marginal distribution and $U(\boldsymbol{z})$.

To model the spatial variability, one needs to account for spatial correlation of different locations in a structure. The correlation between f_c at two locations $\boldsymbol{z}$ and $\boldsymbol{z}'$ is defined by the spatial correlation function $\rho(\boldsymbol{z}, \boldsymbol{z}')$.

When modeling spatial variability of concrete, one can distinguish between two types of spatial variability, related to two different spatial scales. The first type represents the spatial variability at the meso-scale, where the two phases of the concrete are not explicitly considered. Reasons for this type of variability are different concrete batches, local clustering of aggregate or admixtures, decomposition through the vibration procedure, voids and factors related to the construction process. The second type is the micro-scale variability of concrete, which is caused by the composite nature of concrete. The effect of this type of spatial variability is restricted to a small area and wears off relatively fast. Figure 1 illustrates the two types of spatial variability through a potential realization of f_c in a one-dimensional concrete element of $10\,\text{m}$ length (e.g., a core sample). On the one hand, $f_c(z)$ shows fluctuations over short distances due to the micro-scale variability. On the other hand, regions of rather large values of f_c (e.g., on the left side of the plot) and rather small values of f_c (in the center of the plot) can be detected due to the meso-scale variability.
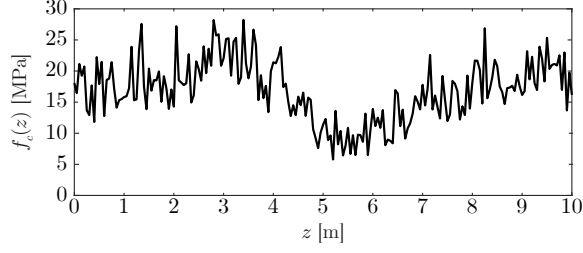
Figure 1: Illustration of the spatial behavior of f_c, combining the effects from micro-scale and meso-scale spatial variability.

As the spatial variability of f_c is affected by micro-scale and meso-scale variability, the correlation function $\rho(\boldsymbol{z}, \boldsymbol{z}')$ needs to consider both effects. This can be done by defining $\rho(\boldsymbol{z}, \boldsymbol{z}')$ as combination of two correlation functions:

$$\rho(\boldsymbol{z}, \boldsymbol{z}') = \gamma_{\mathrm{micro}} \cdot \rho_{\mathrm{micro}}(\boldsymbol{z}, \boldsymbol{z}') + (1 - \gamma_{\mathrm{micro}}) \cdot \rho_{\mathrm{meso}}(\boldsymbol{z}, \boldsymbol{z}'), \tag{4}$$

where $\gamma_{\mathrm{micro}} \in [0, 1]$ is the share of correlation associated with the micro-scale variability, $\rho_{\mathrm{micro}}(\boldsymbol{z}, \boldsymbol{z}')$ and $\rho_{\mathrm{meso}}(\boldsymbol{z}, \boldsymbol{z}')$ are the spatial correlation functions for the micro- and meso-scale variability, respectively. An example of such a correlation model is given in Figure 2. The rapid decrease of $\rho(\boldsymbol{z}, \boldsymbol{z}')$ from 1 to values close to $1 - \gamma_{\mathrm{micro}}$ for small distances $\Delta(\boldsymbol{z}, \boldsymbol{z}')$ between $\boldsymbol{z}$ and $\boldsymbol{z}'$ shows the immediate effect of the micro-scale variability on the spatial correlation. The effect of the meso-scale variability becomes apparent with increasing $\Delta(\boldsymbol{z}, \boldsymbol{z}')$.
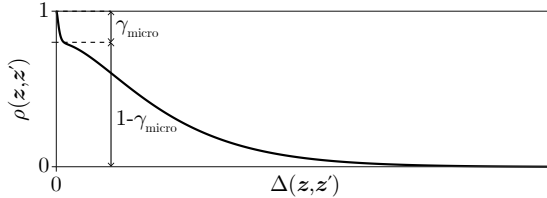

Figure 2: Spatial correlation function $\rho(\boldsymbol{z}, \boldsymbol{z}')$ combining the effect of micro-scale variability and meso-scale variability as function of the spatial distance $\Delta(\boldsymbol{z}, \boldsymbol{z}')$.

Different parametric models exist for the correlation function. We restrict the range of possible correlation models for the meso-scale variability to the Matérn correlation model $\rho_\nu(\boldsymbol{z}, \boldsymbol{z}')$, which is chosen due to its flexibility. It is defined as follows [36, 29]:

$$\rho_\nu(\boldsymbol{z}, \boldsymbol{z}') = \frac{2^{1-\nu}}{\Gamma(\nu)} \left(\sqrt{2\nu} \, \Delta_{\mathrm{w}}(\boldsymbol{z}, \boldsymbol{z}') \right)^\nu K_\nu \left(\sqrt{2\nu} \, \Delta_{\mathrm{w}}(\boldsymbol{z}, \boldsymbol{z}') \right), \tag{5}$$

where $\Gamma(\cdot)$ is the gamma function, $K_\nu(\cdot)$ is the modified Bessel function of the second kind and order ν, and $\Delta_{\mathrm{w}}(\boldsymbol{z}, \boldsymbol{z}')$ is the weighted distance of $\boldsymbol{z}$ and $\boldsymbol{z}'$. In case of an isotropic spatial correlation structure, i.e., all directions are weighted equally, $\Delta_{\mathrm{w}}(\boldsymbol{z}, \boldsymbol{z}') = \frac{\Delta(\boldsymbol{z}, \boldsymbol{z}')}{L_c}$, where $\Delta(\boldsymbol{z}, \boldsymbol{z}')$ is the Euclidean distance $||\boldsymbol{z} - \boldsymbol{z}'||_2$. L_c

7

is the correlation length determining the decrease of the correlation function. Large values of L_c correspond to a slow decay of $\rho_\nu(z, z')$ with increasing $\Delta(z, z')$, whereas small values of L_c indicate a fast decay of $\rho_\nu(z, z')$ with increasing $\Delta(z, z')$. The smoothness of $\rho_\nu(z, z')$ is determined by the smoothness parameter ν. For half-integer values of ν, $\rho_\nu(z, z')$ reduces to the product of an exponential term and a polynomial term [36]. It is noted that for $\nu = \frac{1}{2}$, Equation (5) reduces to the exponential correlation model, whereas for $\nu \to \infty$, it converges to the square-exponential correlation model:

$$\rho_{\frac{1}{2}}(z, z') = \exp\left(-\Delta_{\mathrm{w}}(z, z')\right), \tag{6}$$

$$\rho_\infty(z, z') = \exp\left(-\frac{1}{2}\Delta_{\mathrm{w}}(z, z')^2\right). \tag{7}$$

Concrete structures, especially massive structures, are typically built in blocks or layers. Hence, a transverse anisotropic correlation function is employed to distinguish between spatial directions [37]. This results in different correlation lengths $L_{c,i}$, $i = 1, \ldots d$, where d is the number of spatial dimensions (i.e., 1, 2 or 3). The vector L_c collects all correlation lengths. In this case, $\Delta_{\mathrm{w}}(z, z')$ in Equation (5) is calculated as follows:

$$\Delta_{\mathrm{w}}(z, z') = \sqrt{\sum_{i=1}^{d}\left(\frac{\Delta_i(z, z')}{L_{c,i}}\right)^2}, \tag{8}$$

where $\Delta_i(z, z')$ denotes the spatial distance of z and z' in spatial direction i.

The spatial correlation function $\rho(z, z')$ defines the correlation of any two points $\{z, \ z'\} \in \Omega$ and considers the effect of both the spatial variability on the meso-scale and on the micro-scale. In Section 2.4, we discuss how to employ data in learning the parameters of $\rho(z, z')$. Due to the spatial dimension of
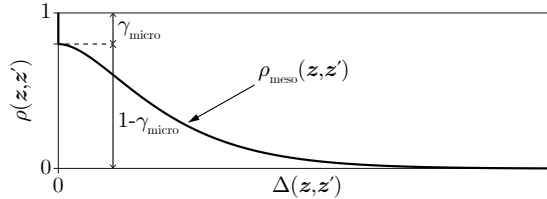

Figure 3: Approximation of spatial correlation function, where the effect of micro-scale variability is approximated by a Dirac function.

the cylindrical specimen, it is impossible to learn the parameters of the micro-scale correlation function $\rho_{\mathrm{micro}}(z, z')$ in practice. However, its exact shape is also not important for predicting the resulting strength of a structure. We therefore propose to approximate the micro-scale correlation by a Dirac delta function and Equation (4) thus reduces to

$$\rho(z, z') = \gamma_{\mathrm{micro}} \cdot \delta_{z,z'} + (1 - \gamma_{\mathrm{micro}}) \cdot \rho_{\mathrm{meso}}(z, z'), \tag{9}$$

8

where $\delta_{\boldsymbol{z},\boldsymbol{z}'}$ is the Dirac delta function returning 1 if $\boldsymbol{z} = \boldsymbol{z}'$ and 0 else. Figure 3 illustrates the approximated correlation function with a jump of $\rho(\boldsymbol{z},\boldsymbol{z}')$ from 1 to $1 - \gamma_{\mathrm{micro}}$ when $\Delta_{\boldsymbol{z},\boldsymbol{z}'} > 0$ to account for the effect of the micro-scale variability on the spatial correlation.

2.3.2. Inter-structure variability

Inter-structure variability leads to uncertainty of the overall material property at a specific structure or site. This uncertainty is at the top level of the hierarchical RF model of the concrete strength f_c [13]. It is modeled by the marginal random field parameters $\boldsymbol{\Theta}$ with joint PDF $f(\boldsymbol{\theta})$. $\boldsymbol{\Theta}$ are the mean and the precision of f_c in a specific structure.

Figure 4 illustrates the hierarchical RF model for the concrete compressive strength $f_c(\boldsymbol{z})$ including the macro-scale variability and the chosen spatial correlation function $\rho(\boldsymbol{z},\boldsymbol{z}')$. Four random realizations of $f_c(\boldsymbol{z})$ are plotted at the bottom of the figure. The corresponding realizations of $\boldsymbol{\Theta}$ and choices of $\rho(\boldsymbol{z},\boldsymbol{z}')$ are indicated in the respective colors.
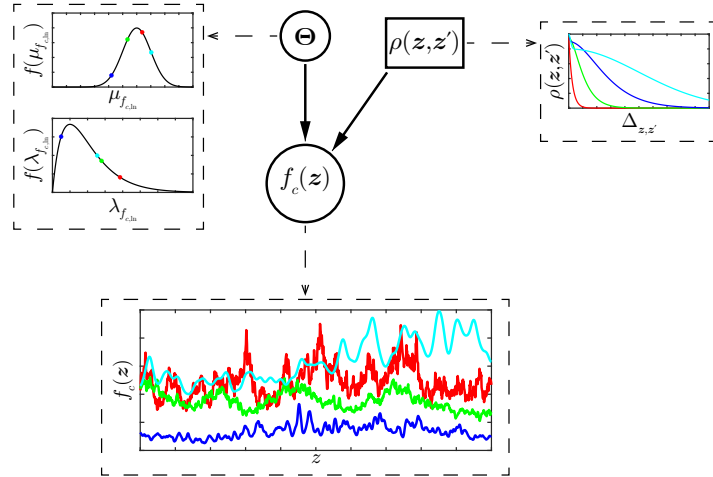

Figure 4: Hierarchical model of the in-situ concrete compressive strength modeled as random field $f_c(\boldsymbol{z})$ with spatial correlation function $\rho(\boldsymbol{z},\boldsymbol{z}')$. The four colors correspond to four random realizations of $f_c(\boldsymbol{z})$ and $f_c(\boldsymbol{z})$ and choices of $\rho(\boldsymbol{z},\boldsymbol{z}')$.

2.4. Learning the random field model from data

Measurements of the in-situ concrete strength form an important part of structural verification of existing structures. Although non-destructive test techniques can be used to get indirect measurements of the concrete strength (e.g., testing with a rebound hammer [38] or measurements of the ultrasonic pulse velocity [39]), the most accurate results are obtained by taking core samples from the structure and directly testing the concrete strength of standardized cylindrical specimen [6, 7]. Especially for the verification of existing massive concrete structures, taking core samples is essential for getting detailed information on the concrete

properties [40]. The number of core samples as well as their orientation depends on the investigated structure and the aim of the investigation [8, 7]. Standardized specimen are visually selected from the available drilling cores before being extracted, prepared and tested to determine their concrete compressive strength.

2.4.1. Data uncertainty

In-situ data is subject to uncertainty associated with the measured value (measurement uncertainty) and - if the measurements are not properly documented - the location of the measurement (position uncertainty).

There are different sources of measurement uncertainty; some are related to the measurement procedure (e.g., the laboratory operator or the measurement device [11]), others stem from an underlying transformation (e.g., when inferring the splitting tensile strength via the indirect tensile strength test [41] or from the conversion of cylindrical core samples with small diameters [7]). Contrary to the field of geotechnical engineering, where probabilistic models have been developed to account for this measurement uncertainty [e.g., 42], only little attention is paid to it in structural engineering applications. The measurement outcomes of concrete samples from drilling cores are typically set equal to the in-situ concrete parameters, as long as the test specimen fulfills certain requirements [7]. The only exception to this rule is the case of outliers, which are eliminated using outlier tests [e.g., 43, 44].

The main reason for position uncertainty is the lack of documentation, since information about the exact measurement location is not required in standard methods for estimating characteristic values [3, 7, 8]. Position uncertainty can hinder the applicability of a spatial analysis.

2.4.2. Bayesian random field update

The hierarchical RF model of Section 2.3 forms the basis for explicitly including the spatial locations of the data in learning the distribution parameters and the predictive spatial distribution of f_c. In the following, we summarize a Bayesian approach to learn the RF and its parameters based on [22]. The approach reduces to the Bayesian approach for calculating characteristic values in [3] for specific parameter choices [22].

It is assumed that measurement data $\mathbf{M}$ is available from cylindrical specimen extracted from core samples of an existing concrete structure. $\mathbf{M} = [\boldsymbol{x}_m, \mathbf{Z}_m]$, where $\boldsymbol{x}_m = [x_{m,1}, x_{m,2}, \ldots, x_{m,n}]^\mathsf{T}$ are the n_m measurement outcomes and $\mathbf{Z}_m = [\boldsymbol{z}_{m,1}, \boldsymbol{z}_{m,2}, \ldots, \boldsymbol{z}_{m,n}]^\mathsf{T}$ the corresponding locations. Figure 5 extends the hierarchical RF model of Figure 4 by including the data $\mathbf{M}$ associated with measurement uncertainty ε.

Due to the hierarchical modeling approach, the updating needs to be done in two steps. The data $\mathbf{M}$ is included in a first step to update the distribution of $\boldsymbol{\Theta}$, by application of Bayes' rule [21]:

$$f(\boldsymbol{\theta}|\mathbf{M}) \propto f(\boldsymbol{\theta}) \cdot \mathrm{L}(\boldsymbol{\theta}|\mathbf{M}), \tag{10}$$

where $f(\boldsymbol{\theta})$ is the prior distribution of $\boldsymbol{\Theta}$ and $f(\boldsymbol{\theta}|\mathbf{M})$ is the posterior distribution of $\boldsymbol{\Theta}$ given the data $\mathbf{M}$, which enters the model via the likelihood function $\mathrm{L}(\boldsymbol{\theta}|\mathbf{M})$. $f(\boldsymbol{\theta}|\mathbf{M})$ can then be used in a second
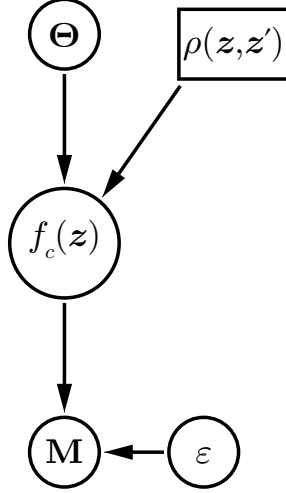
10

Figure 5: Hierarchical random field model for learning the in-situ concrete compressive strength $f_c(\boldsymbol{z})$ from data $\mathbf{M}$ of standardized cylindrical samples taken from the structure. The measurements in $\mathbf{M}$ are associated with measurement uncertainty ε.

updating step to find the spatial posterior predictive distribution of $f_c(\boldsymbol{z})$. In the general case, the posterior distribution in Equation (10) needs to be approximated numerically, e.g., through Markov chain Monte Carlo (MCMC) methods [e.g., 45]. For certain cases, however, closed-form expressions can be found for updating the hierarchical RF model. The following modeling choices are made in order to enable such a closed-form update [46, 9, 22]:

i) The marginal distribution of $f_c(\boldsymbol{z})$ is a lognormal distribution. Then, $f_{c,\ln}(\boldsymbol{z}) = \ln(f_c(\boldsymbol{z}))$ follows a normal distribution with mean function $\mu_{f_{c,\ln}}(\boldsymbol{z})$ and precision function $\lambda_{f_{c,\ln}}(\boldsymbol{z})$. The hierarchical modeling and updating process is done for the corresponding RF $f_{c,\ln}(\boldsymbol{z})$, a Gaussian RF completely defined by its spatial functions for the mean $\mu_{f_{c,\ln}}(\boldsymbol{z})$, the precision $\lambda_{f_{c,\ln}}(\boldsymbol{z})$ and the autocorrelation function $\rho(\boldsymbol{z}, \boldsymbol{z}')$ (cf. Section 2.3.1).

ii) Before including site-specific information, $f_{c,\ln}(\boldsymbol{z})$ is assumed to be homogeneous, i.e., the spatial moments are space-invariant and the spatial correlation is a function of the difference in location. That is, $\mu_{f_{c,\ln}}(\boldsymbol{z}) = \mu_{f_{c,\ln}} \ \forall \ \boldsymbol{z} \in \Omega$ and $\lambda_{f_{c,\ln}}(\boldsymbol{z}) = \lambda_{f_{c,\ln}} \ \forall \ \boldsymbol{z} \in \Omega$. $\rho(\boldsymbol{z}, \boldsymbol{z}')$ is defined according to Equation (9) with $\rho_{\mathrm{meso}}(\boldsymbol{z}, \boldsymbol{z}')$ given by the Matérn model of Equation (5).

iii) The prior distribution of $\boldsymbol{\Theta} = [\mu_{f_{c,\ln}}, \lambda_{f_{c,\ln}}]^{\mathsf{T}}$, $f(\boldsymbol{\theta})$ is modeled with a normal-gamma ($\mathcal{NG}$) distribution, where $\lambda_{f_{c,\ln}}$ follows a gamma distribution and $\mu_{f_{c,\ln}}$ follows a normal distribution conditional on $\lambda_{f_{c,\ln}}$[9].

iv) The measurement uncertainty is defined through a multiplicative error, i.e., the measurement outcome

11

$f_{c,m,i}$ at location $\boldsymbol{z}_{m,i}$ is given as

$$f_{c,m,i} = f_c(\boldsymbol{z}_{m,i}) \cdot \varepsilon_i. \tag{11}$$

The ε_i are modeled as independent lognormal random variables with median 1. To retain the analytical form of the update, it is necessary to account for the measurement error in the correlation function. This results in a modified correlation function that takes an identical form as Equation (9), i.e,

$$\rho_{\mathrm{mod}}(\boldsymbol{z}, \boldsymbol{z}') = \gamma \cdot \delta_{\boldsymbol{z}, \boldsymbol{z}'} + (1 - \gamma) \cdot \rho_{\mathrm{meso}}(\boldsymbol{z}, \boldsymbol{z}'), \tag{12}$$

where $\gamma \in [0, 1]$ lumps the contribution of both micro-scale variability and measurement error into a single factor [22]. $\gamma = \gamma_{\mathrm{micro}} + \gamma_\varepsilon - \gamma_{\mathrm{micro}}\gamma_\varepsilon$, where $\gamma_\varepsilon \in [0, 1]$ is the contribution of the measurement error. We work with the lumped factor γ because a distinction of the contribution of the individual effects is not possible based on spatial data.

Using the assumptions above, the posterior predictive RF for $f_c(\boldsymbol{z})$ has log-Student's t-marginal distribution [47]. A log-Student's t-RF is parameterized in terms of the spatial functions for the parameters of the underlying Student's t-RF given by the following equations [22]:

$$\mu_t(\boldsymbol{z}) = \mu_n + \boldsymbol{R}_{\boldsymbol{z},m}\mathbf{R}_m^{-1}(\boldsymbol{x}_m - \mu_n \mathbf{1}_n)^\mathsf{T}, \tag{13}$$

$$\lambda_t(\boldsymbol{z}_1, \boldsymbol{z}_2) = \frac{\alpha_n}{\beta_n} \left(\rho(\boldsymbol{z}_1, \boldsymbol{z}_2) - \boldsymbol{R}_{\boldsymbol{z}_1,m}\mathbf{R}_m^{-1}\boldsymbol{R}_{\boldsymbol{z}_2,m}^\mathsf{T} + (1 - \boldsymbol{R}_{\boldsymbol{z}_1,m}\mathbf{R}_m^{-1}\mathbf{1}_n^\mathsf{T})\kappa_n^{-1}(1 - \boldsymbol{R}_{\boldsymbol{z}_2,m}\mathbf{R}_m^{-1}\mathbf{1}_n^\mathsf{T}) \right)^{-1}, \tag{14}$$

$$\nu_t = 2\alpha_n. \tag{15}$$

$\boldsymbol{R}_{\boldsymbol{z},m} : \mathbb{R}^d \to \mathbb{R}^{1 \times n_m}$ is a row vector function with element i defined as $\rho_{\mathrm{mod}}(\boldsymbol{z}, \boldsymbol{z}_{m,i})$ and the parameters μ_n, κ_n, α_n and β_n are given as [22]

$$\mu_n = \frac{\kappa_0 \mu_0 + \mathbf{1}_n \mathbf{R}_m^{-1} \boldsymbol{x}_m^\mathsf{T}}{\kappa_0 + \mathbf{1}_n \mathbf{R}_m^{-1} \mathbf{1}_n^\mathsf{T}}, \tag{16}$$

$$\kappa_n = \kappa_0 + \mathbf{1}_n \mathbf{R}_m^{-1} \mathbf{1}_n^\mathsf{T}, \tag{17}$$

$$\alpha_n = \alpha_0 + \frac{n_m}{2}, \tag{18}$$

$$\beta_n = \beta_0 + \frac{1}{2} \left(\boldsymbol{x}_m \mathbf{R}_m^{-1} \boldsymbol{x}_m^\mathsf{T} + \frac{\kappa_0 \mu_0^2 \mathbf{1}_n \mathbf{R}_m^{-1} \mathbf{1}_n^\mathsf{T} - 2\kappa_0 \mu_0 \mathbf{1}_n \mathbf{R}_m^{-1} \boldsymbol{x}_m^\mathsf{T} - (\mathbf{1}_n \mathbf{R}_m^{-1} \boldsymbol{x}_m^\mathsf{T})^2}{\kappa_0 + \mathbf{1}_n \mathbf{R}_m^{-1} \mathbf{1}_n^\mathsf{T}} \right). \tag{19}$$

$\mathbf{1}_n$ denotes a $1 \times n_m$-vector of ones and $\mathbf{R}_m$ is the $n_m \times n_m$ correlation matrix of the measurement locations, where element (i, j) is defined as $\rho_{\mathrm{mod}}(\boldsymbol{z}_{m,i}, \boldsymbol{z}_{m,j})$. μ_0, κ_0, α_0 and β_0 are the parameters of the prior $\mathcal{NG}$ distribution $f(\boldsymbol{\theta})$. The Appendix gives the PDF and CDF of the log-Student's t-distribution.

2.4.3. Learning the correlation model

The closed-form update in Section 2.4.2 is valid for a fixed correlation function $\rho_{\mathrm{mod}}(\boldsymbol{z}, \boldsymbol{z}')$. However, $\rho_{\mathrm{mod}}(\boldsymbol{z}, \boldsymbol{z}')$ is typically not known in practical applications and, hence, is treated as uncertain model input with parameter vector $\mathbf{T}$. $\mathbf{T} = [\gamma, \nu, \boldsymbol{L_c}]$ includes the meso-scale (with the transverse anisotropic Matérn model) and micro-scale variability (approximated by a Dirac function) for the hierarchical RF model (cf. Section 2.3.1) as well as the measurement uncertainty ε, which is included in $\rho_{\mathrm{mod}}(\boldsymbol{z}, \boldsymbol{z}')$ through γ. Figure 6 illustrates the extended hierarchical RF model when the parameters of $\rho_{\mathrm{mod}}(\boldsymbol{z}, \boldsymbol{z}')$ are treated as random vector.
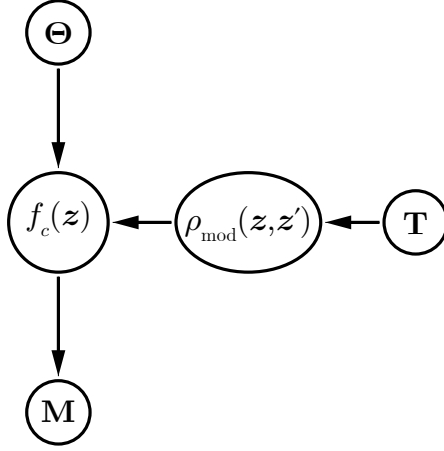

Figure 6: Hierarchical random field model for learning the in-situ concrete compressive strength $f_c(\boldsymbol{z})$ from data $\mathbf{M}$ with uncertain correlation model $\rho_{\mathrm{mod}}(\boldsymbol{z}, \boldsymbol{z}')$ with model parameters $\mathbf{T}$.

Bayes' theorem can be used to learn the posterior distribution of the correlation parameters from the data:

$$f(\boldsymbol{\tau}|\mathbf{M}) \propto f(\boldsymbol{\tau}) \cdot f(\mathbf{M}|\boldsymbol{\tau}). \tag{20}$$

The specific model choices of Section 2.4.2 lead to the following expression for $f(\boldsymbol{\tau}|\mathbf{M})$ [22]:

$$f(\mathbf{M}|\boldsymbol{\tau}) = \left(\frac{\kappa_0}{\kappa_n(\boldsymbol{\tau})}\right)^{\frac{1}{2}} \frac{\Gamma(\alpha_n)\beta_0^{\alpha_0}}{\Gamma(\alpha_0)(\beta_n(\boldsymbol{\tau}))^{\alpha_n}} (2\pi)^{-\frac{n}{2}} \det(\mathbf{R}_m(\boldsymbol{\tau}))^{-\frac{1}{2}}, \tag{21}$$

where $\kappa_n(\boldsymbol{\tau})$, α_n, $\beta_n(\boldsymbol{\tau})$ and $\mathbf{R}_m(\boldsymbol{\tau})$ follow the definitions in Section 2.4.2 conditional on the chosen correlation model parameters.

The maximum a-posteriori (MAP) estimate can be employed to learn a point estimate of the correlation parameters from the data $\mathbf{M}$ [48]. That is, instead of inferring the full posterior distribution $f(\boldsymbol{\tau}|\mathbf{M})$, it is approximated by its mode, $\boldsymbol{\tau}^*$. This is done by solving the following optimization problem [22]:

$$\boldsymbol{\tau}^* = \arg\min_{\boldsymbol{\tau} \in \mathbf{T}} \ln(\kappa_n(\boldsymbol{\tau})) + 2\alpha_n \ln(\beta_n(\boldsymbol{\tau})) + \ln(\det(\mathbf{R}_m(\boldsymbol{\tau}))) - 2\ln(f(\boldsymbol{\tau})), \tag{22}$$

13

where $f(\boldsymbol{\tau})$ is the prior distribution of $\mathbf{T}$. $\boldsymbol{\tau}^*$ is equivalent to the maximum likelihood estimate of $\mathbf{T}$ in the case of a uniform prior distribution $f(\boldsymbol{\tau})$ [49]. After selecting the correlation model, the RF model can be learned from $\mathbf{M}$ as described in Section 2.4.2.

Alternatively, the posterior mean $\boldsymbol{\mu}_{\mathbf{T}|\mathbf{M}}$ can be used as an approximation for $\mathbf{T}$ given $\mathbf{M}$. Unlike the MAP estimate, the posterior mean is not dominated by local extrema of the posterior distribution. Given $n_{\mathbf{T}}$ unknown correlation parameters in the vector $\mathbf{T}$, the marginal posterior mean of $T_i,\ i=1,\dots,n_{\mathbf{T}}$ is given as

$$\mu_{T_i|\mathbf{M}} = \mathrm{E}\left[T_i|\mathbf{M}\right] = \frac{1}{\mathcal{C}_{\mathbf{T}}} \int_{\mathbf{T}} \tau_i f(\boldsymbol{\tau}) f(\mathbf{M}|\boldsymbol{\tau}) \mathrm{d}\boldsymbol{\tau}, \tag{23}$$

where $\mathcal{C}_{\mathbf{T}}$ is the following normalization constant:

$$\mathcal{C}_{\mathbf{T}} = \int_{\mathbf{T}} f(\boldsymbol{\tau}) f(\mathbf{M}|\boldsymbol{\tau}) \mathrm{d}\boldsymbol{\tau}. \tag{24}$$

If a point-estimate of $\mathbf{T}$ is not sufficient, the analytical update to learn the posterior predictive model for the concrete strength is not sufficient. However, it can be approximated numerically, e.g., by means of MCMC algorithms [45]. The analytical update is employed in generating samples from $f(\boldsymbol{\tau}|\mathbf{M})$, which are then used to approximate the posterior predictive distribution. The point-wise marginal posterior predictive PDF $f(f_{c,\boldsymbol{z}}|\mathbf{M}),\ \boldsymbol{z}\in\Omega$ can be approximated as follows:

$$f(f_{c,\boldsymbol{z}}|\mathbf{M}) \approx \frac{1}{N_{MCMC}} \sum_{i=1}^{N_{MCMC}} f(f_{c,\boldsymbol{z}}|\mathbf{M},\boldsymbol{\tau}_i), \tag{25}$$

where N_{MCMC} is the sample size in the MCMC algorithm and $\boldsymbol{\tau}_i,\ i=1,\dots,N_{MCMC}$ are samples from $f(\boldsymbol{\tau}|\mathbf{M})$. The posterior predictive CDF can be approximated accordingly:

$$F(f_{c,\boldsymbol{z}}|\mathbf{M}) \approx \frac{1}{N_{MCMC}} \sum_{i=1}^{N_{MCMC}} F(f_{c,\boldsymbol{z}}|\mathbf{M},\boldsymbol{\tau}_i). \tag{26}$$

The evaluation of $F(f_{c,\boldsymbol{z}}|\mathbf{M})$ requires the analytical Bayesian update for each of the N_{MCMC} samples. Using the model assumptions of Section 2.4.2, $F(f_{c,\boldsymbol{z}}|\mathbf{M},\boldsymbol{\tau}_i)$ is the CDF of the log-Student's t-distribution (cf. Appendix).

2.4.4. Choosing the prior normal-gamma distribution parameters from data

The parameters of the prior distribution should be chosen based on expertise and literature, or selected as a non-informative prior. Alternatively, the prior parameters can be determined from available data from similar structures, which are not part of the analysis at hand. We suggest to employ maximum likelihood estimation (MLE) to estimate these prior parameters, specifically the parameters $\mu_0,\ \kappa_0,\ \alpha_0$ and β_0 of the prior $\mathcal{NG}$ distribution $f(\boldsymbol{\theta})$. Here we consider data sets from n_{MLE} structures, each set consisting of n_i

14

measurements of f_c at the specific structure i. The following sample estimators are calculated for each data set:

$$\bar{\mu}_i = \frac{1}{n_i} \sum_{j=1}^{n_i} \ln\left(f_{c,m,j}\right),$$ (27)

$$\bar{\lambda}_i = \left(\frac{1}{n_i - 1} \sum_{j=1}^{n_i} \left(\ln\left(f_{c,m,j}\right) - \bar{\mu}_i\right)^2\right)^{-1}.$$ (28)

They are used to define the following:

$$\bar{\boldsymbol{\mu}} = [\bar{\mu}_1, \ldots, \bar{\mu}_{n_{\mathrm{MLE}}}],$$ (29)

$$\bar{\boldsymbol{\lambda}} = [\bar{\lambda}_1, \ldots, \bar{\lambda}_{n_{\mathrm{MLE}}}],$$ (30)

$$\bar{\boldsymbol{\Lambda}} = \mathrm{diag}\left(\bar{\boldsymbol{\lambda}}\right).$$ (31)

$\bar{\boldsymbol{\Lambda}}$ is a diagonal matrix with the entries of $\bar{\boldsymbol{\lambda}}$ on the main diagonal and zeros elsewhere.

The MLE estimators for the prior $\mathcal{NG}$ distribution are then given as [50, 9]:

$$\hat{\mu}_0 = \frac{\mathbf{1}\bar{\boldsymbol{\Lambda}}\bar{\boldsymbol{\mu}}^{\mathsf{T}}}{\mathbf{1}\bar{\boldsymbol{\Lambda}}\mathbf{1}^{\mathsf{T}}},$$ (32)

$$\hat{\kappa}_0 = \frac{n_{\mathrm{MLE}}}{(\bar{\boldsymbol{\mu}} - \hat{\mu}_0 \mathbf{1})\bar{\boldsymbol{\Lambda}}(\bar{\boldsymbol{\mu}} - \hat{\mu}_0 \mathbf{1})^{\mathsf{T}}},$$ (33)

$$\hat{\alpha}_0 = \Psi^{-1}\left(\ln\left(\hat{\beta}_0\right) + \frac{1}{n_{\mathrm{MLE}}} \sum_i^{n_{MLE}} \ln\left(\bar{\lambda}_i\right)\right),$$ (34)

$$\hat{\beta}_0 = \frac{n_{\mathrm{MLE}} \cdot \hat{\alpha}_0}{\mathbf{1}\bar{\boldsymbol{\Lambda}}\mathbf{1}^{\mathsf{T}}}.$$ (35)

$\mathbf{1}$ denotes a $1 \times n_{\mathrm{MLE}}$-vector of ones and $\Psi^{-1}(\cdot)$ is the inverse digamma function. $\hat{\alpha}_0$ and $\hat{\beta}_0$ have to be found iteratively, since both parameters appear in Equation (34) and in Equation (35).

The MLE estimators in Equations (32) to (35) are only valid under the assumption that f_c conditional on $\boldsymbol{\Theta}$ follows a lognormal distribution. They do not account for potential correlation among the measurements in the available data sets and can only be applied if $n_{\mathrm{MLE}} > 1$. The spatial update of Section 2.4.2 is directly applicable after replacing the prior $\mathcal{NG}$ distribution parameters by the respective MLE estimates.

Sometimes, site-specific data (e.g., from previous investigations on the structure) is available but the measurement locations are not documented, as this information is not needed in the standard methods to learn the characteristic values of the concrete strength [3, 7, 8]. Such data can be included in the above MLE procedure for learning the prior $\mathcal{NG}$ distribution parameters.

2.4.5. Bayesian learning of random field parameters without site-specific data

If no site-specific data is available, but data from similar structures (and site-specific data without measurement locations) can be used, one can still set up an RF model. Based on the MLE estimators in Equations (32) to (35), the predictive RF has log-Student's t-marginal distribution and is parameterized in terms of the parameters of the underlying Student's t-RF. Unlike the case where the spatial location of the measurements is available, the predictive RF is a homogeneous RF with parameters given by

$$\mu_t = \hat{\mu}_0, \tag{36}$$

$$\lambda_t(\boldsymbol{z}_1, \boldsymbol{z}_2) = \frac{\hat{\alpha}_0}{\hat{\beta}_0} \left(\rho_{\mathrm{mod}}(\boldsymbol{z}_1, \boldsymbol{z}_2) + \hat{\kappa}_0^{-1} \right)^{-1}, \tag{37}$$

$$\nu_t = 2\hat{\alpha}_0. \tag{38}$$

The parameters obtained in this way define the prior predictive RF, since the model is learned without site-specific information, and can be used for predictions about the spatially variable quantity [21].

3. Data analysis

This section applies the proposed methodology to learn a spatial model for the compressive strength of two ship lock chamber walls. The data analysis serves to investigate and demonstrate the proposed model, shows possible correlation models for specific structures and highlights challenges with the proposed approach encountered in practice.

The considered walls were built in layers of tamped concrete and, thus, show significant anisotropic behavior [40, 22]. A transverse anisotropic correlation function, distinguishing between horizontal (z_1, z_2) and vertical (z_3) distances is employed to account for this behavior. The resulting $\Delta_{\mathrm{w}}(\boldsymbol{z}, \boldsymbol{z}')$ is given by

$$\Delta_{\mathrm{w}}(\boldsymbol{z}, \boldsymbol{z}') = \sqrt{\left(\frac{\Delta_h(\boldsymbol{z}, \boldsymbol{z}')}{L_{c,h}} \right)^2 + \left(\frac{\Delta_v(\boldsymbol{z}, \boldsymbol{z}')}{L_{c,v}} \right)^2}, \tag{39}$$

where $\Delta_h(\boldsymbol{z}, \boldsymbol{z}')$ and $\Delta_v(\boldsymbol{z}, \boldsymbol{z}')$ denote the horizontal and vertical distance respectively between $\boldsymbol{z}$ and $\boldsymbol{z}'$. $L_{c,h}$ and $L_{c,v}$ denote the horizontal and vertical correlation lengths.

The vector $\mathbf{T}$ of correlation parameters is treated as random vector and learned from the data. However, the prior information on the elements in $\mathbf{T}$ is vague, which makes the choice of a prior distribution a challenging task. Hence, the multivariate uniform distribution on the domain of definition is chosen as prior distribution. The measurement uncertainty is acounted for in the correlation function through the factor γ.

3.1. Ship lock Oldenburg

This case study investigates the ship lock at the river Hunte in Oldenburg, Germany. It was built in the 1920s from unreinforced tamped concrete. The chamber has a length of 128 m and a usable width of

12 m between the chamber walls. During an extensive repair in 1983, the upper 2 m of the chamber walls were replaced by reinforced concrete. The focus of this study is the original concrete of one of the chamber walls, for which strength measurements are available at three vertical core samples from an investigation in 2014. Figure 7 shows a front view and the cross section of the chamber wall with the two concrete layers of different age and the position of the core samples. Table 1 lists the 24 measurements of the concrete compressive strength and their corresponding measurement location in z_1 and z_3 ($z_2 = -1.0$ m for all 24 measurements).
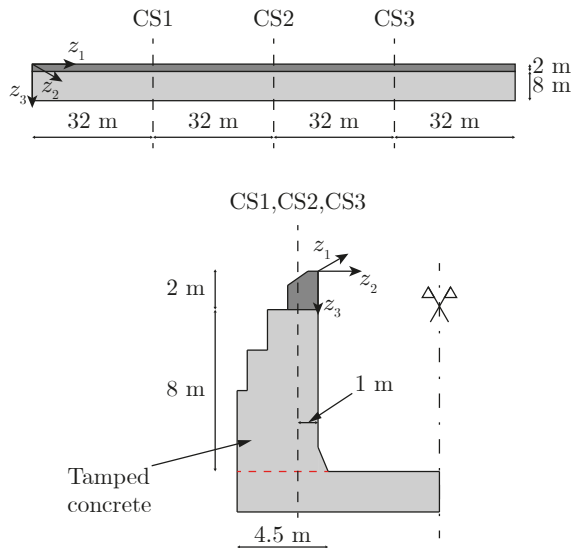
Figure 7: Front view (top) and cross section (bottom) of the ship lock wall in Oldenburg including the locations of three vertical core samples (CS1, CS2 and CS3), from which 24 measurements of the concrete compressive strength have been taken. Tamped concrete is indicated in light grey, reinforced concrete is shown in dark grey.

The prior parameters for the $\mathcal{NG}$ distribution $f(\boldsymbol{\theta})$ are chosen as follows:

$$[\mu_0, \kappa_0, \alpha_0, \beta_0] = \left[/, 0, -\frac{1}{2}, 0\right], \tag{40}$$

which gives the non-informative prior distribution $f(\boldsymbol{\theta}) = \lambda_X^{-1}$ [46, 22].

3.1.1. Learning the correlation model

The correlation model contains four unknown parameters, namely the two correlation lengths, the parameter for the micro-scale variability and the smoothness parameter of the Matérn corrrelation model. The 24 measurements are not sufficient to learn all parameters without the support from an informative prior distribution. Thus, the Matérn smoothness parameter is set to $\nu = 0.5$, corresponding to the exponential correlation model. In addition, the parameter for the micro-scale variability γ is not learned from the data either. Instead, the analysis is carried out for different values of γ.

17

Table 1: Measurements of the concrete compressive strength obtained from three core samples in the north wall of the ship lock Oldenburg. The locations of the core samples are indicated in Figure 7.

CS1		CS2		CS3	
$(z_1 = 32.00\,\mathrm{m})$		$(z_1 = 64.00\,\mathrm{m})$		$(z_1 = 96.00\,\mathrm{m})$	
z_3	$f_{c,m}$	z_3	$f_{c,m}$	z_3	$f_{c,m}$
[m]	[N mm^{-2}]	[m]	[N mm^{-2}]	[m]	[N mm^{-2}]
2.40	29.2	2.21	21.2	2.34	18.5
3.24	15.5	3.25	16.0	3.34	10.3
4.25	8.7	4.05	32.0	4.17	13.2
5.15	12.3	5.33	20.7	5.24	14.5
6.12	16.2	6.15	13.8	6.27	25.4
7.33	11.6	7.25	12.1	7.12	14.5
8.15	13.4	8.40	8.6	8.23	13.2
9.05	13.9	9.45	14.8	9.08	33.0

The correlation length estimates are obtained via a solution of the optimization problem of Equation (22) resulting in the following MAP estimates for $L_{c,h}$ and $L_{c,v}$:

$$\gamma = 0.1: \quad \left[L_{c,h}^*,\ L_{c,v}^*\right] = [2.08\,\mathrm{m},\ 0.62\,\mathrm{m}], \tag{41}$$

$$\gamma = 0.3: \quad \left[L_{c,h}^*,\ L_{c,v}^*\right] = [2.70\,\mathrm{m},\ 0.71\,\mathrm{m}], \tag{42}$$

$$\gamma = 0.5: \quad \left[L_{c,h}^*,\ L_{c,v}^*\right] = [3.75\,\mathrm{m},\ 0.87\,\mathrm{m}]. \tag{43}$$

From these values, it appears that an increase in the micro-scale variability leads to an increase in the MAP estimates of the correlation lengths. Large correlation lengths correspond to RFs with smooth spatial variability, while small correlation lengths indicate a highly fluctuating RF. When γ is large, a large portion of the variability observed in the data is attributed to the micro-scale variability (and the measurement uncertainty). In this case, a smaller part of the data variability is attributed to spatial variability and the associated correlation length is larger. To illustrate this, the posterior distribution of the two correlation lengths is plotted in Figure 8 for varying γ. The respective MAP estimates of $\boldsymbol{L_c}$ are indicated by blue dots. In panel a, the micro-scale variability only plays a minor role for the overall variability ($\gamma = 0.1$), leading to a clear mode of the posterior distribution $f(\boldsymbol{L_c}|\mathbf{M}, \gamma)$. Increasing the influence of the micro-scale variability flattens the posterior distribution and shifts the mode towards larger values for the correlation lengths, as can be seen in panels b ($\gamma = 0.3$) and c ($\gamma = 0.5$). All three panels show an additional local maximum of $f(\boldsymbol{L_c}|\mathbf{M}, \gamma)$ in the bottom right corner, i.e., in regions of large $L_{c,h}$ and small $L_{c,v}$. This behavior is caused by the local horizontal clustering of the measurements in three vertical core samples, whereas they

18

are approximately evenly distributed in vertical direction. Such an arrangement reduces the learning effect for $L_{c,h}$ and makes $f(\boldsymbol{L_c}|\mathbf{M},\gamma)$ more sensitive to changes in $L_{c,v}$.
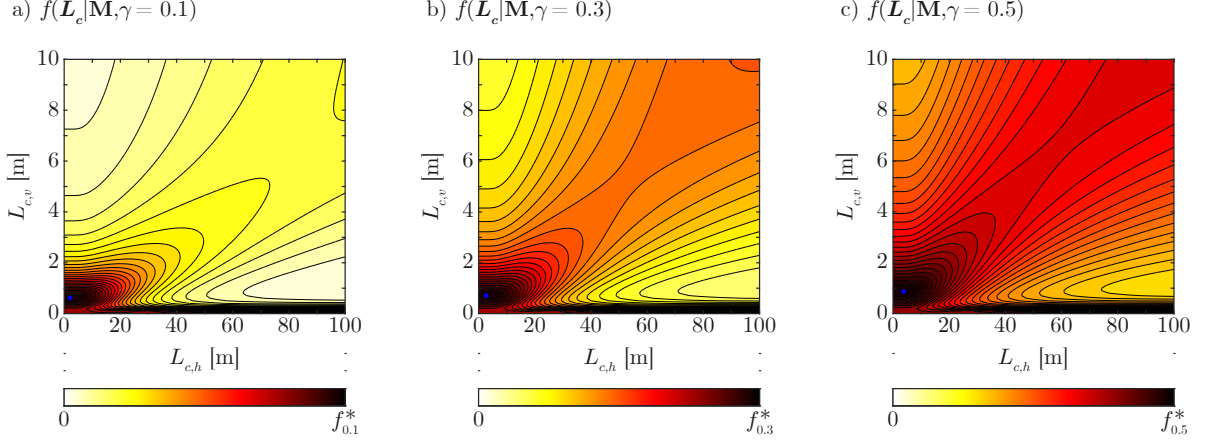

Figure 8: Posterior distribution of the correlation lengths in horizontal ($L_{c,h}$) and vertical ($L_{c,v}$) direction for $\nu = 0.5$ and varying values of γ. The blue dots indicate the MAP estimates at the respective modes of the posterior distribution. $f_{0.1}^*$, $f_{0.3}^*$ and $f_{0.5}^*$ are the values of $f(\boldsymbol{L_c}|\mathbf{M},\gamma)$ at the respective distribution modes.

3.1.2. Spatial posterior predictive concrete compressive strength

The Bayesian RF update is used to learn the posterior predictive random field of the concrete compressive strength. The following posterior $\mathcal{NG}$ distribution parameters are calculated from Equations (16) to (19):

$$\gamma = 0.1 : \quad [\mu_n, \kappa_n, \alpha_n, \beta_n] = [2.76,\ 17.27,\ 11.5,\ 1.61]\,, \tag{44}$$

$$\gamma = 0.3 : \quad [\mu_n, \kappa_n, \alpha_n, \beta_n] = [2.76,\ 17.30,\ 11.5,\ 1.59]\,, \tag{45}$$

$$\gamma = 0.5 : \quad [\mu_n, \kappa_n, \alpha_n, \beta_n] = [2.76,\ 17.33,\ 11.5,\ 1.59]\,. \tag{46}$$

Since α_n only depends on the number of measurements, it is constant for any choice of γ. Although the other three $\mathcal{NG}$ distribution parameters depend on the spatial correlation of the measurements, they differ only slightly for different choices of γ. This is due to the fact that an increase in γ automatically decreases the spatial correlation of two locations in the random field (cf. Equation (4)) and, thus, compensates the increased spatial correlation of the measurement locations that comes with larger correlation lengths.

The random field parameters can be determined by application of Equations (13) to (15). With these parameters, the spatial characteristic value $f_{c,\mathrm{k}}(\boldsymbol{z})$ can be determined as the $5\%-$quantile value of the log-Student's t-RF. It is illustrated in Figure 9 for the $z_1 - z_3$ plane in which the core samples have been taken. While $f_{c,\mathrm{k}}(\boldsymbol{z})$ is strongly influenced by the measurement values in regions close to the measurement locations, one can see convergence to a global value in regions away from the measurements. It is noted

that the extreme values of $f_{c,k}(z)$ are located in the illustrated $z_1 - z_3$ plane, the point-wise values tend towards the global value for a shift in z_2. The effect of a variation in γ on the global characteristic value is negligible, as it is $8.2\,\text{MPa}$ for all three cases. The global characteristic value appears in regions without spatial correlation to the measurement locations and, thus, is determined by the posterior parameters of the $\mathcal{NG}$ distribution. Those parameters are almost constant for all three choices of γ, leading to a similar global characteristic value. Using the standardized Bayesian approach of EN 1990 with the 24 measurements from Table 1 leads to a space-invariant characteristic value of $f_{c,k,EN} = 8.4\,\text{MPa}$, i.e., it is slightly higher than the global characteristic value obtained with the spatial model.

The effect of the different values of $\boldsymbol{L_c}$ can be seen in Figure 9 by comparing the regions of the wall where $f_{c,k}(z)$ differs from the global value. In panel a, the spatial effect of the measurement locations is restricted to regions close to the core sample locations, while these regions become larger in panels b and c, where $\boldsymbol{L_c}$ takes larger values.
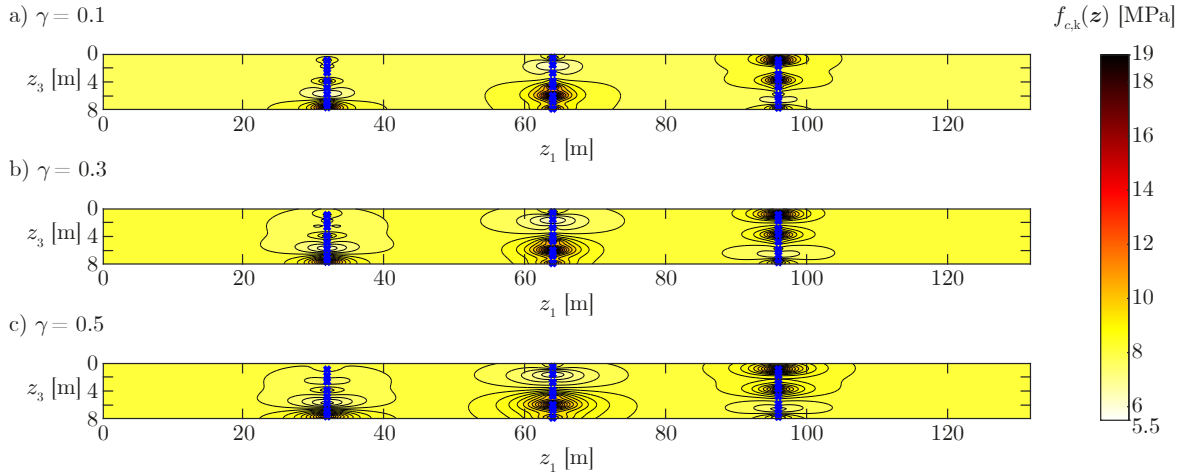

Figure 9: Spatial characteristic value $f_{c,k}(z)$ of the posterior predictive random field for different choices of γ.

3.1.3. Effect of an informative prior distribution

In addition to the 24 measurements of Table 1, three data sets are available, one from previous investigations on the same ship lock and two from similar ship locks (one of which is analyzed in Section 3.2). The following sample moments are used to obtain the MLE estimates of the prior $\mathcal{NG}$ parameters (cf. Equations (27) to (30)):

$$\bar{\boldsymbol{\mu}} = [2.83, \ 2.12, \ 2.03], \tag{47}$$

$$\bar{\boldsymbol{\lambda}} = [3.50, \ 3.78, \ 2.53]. \tag{48}$$

20

From these, the prior $\mathcal{NG}$ parameters are estimated:

$$[\hat{\mu}_0, \ \hat{\kappa}_0, \ \hat{\alpha}_0, \ \hat{\beta}_0] = [2.35, \ 2.37, \ 34.52, \ 10.56]. \tag{49}$$

Using an informative prior distribution reduces the uncertainty in the RF parameters and therefore also affects the posterior estimates of the spatial correlation structure. Setting $\gamma = 0.1$, the following MAP estimates for $L_{c,h}$ and $L_{c,v}$ are obtained:

$$\left[L_{c,h}^*, \ L_{c,v}^*\right] = [33.33 \, \text{m}, \ 2.49 \, \text{m}]. \tag{50}$$

Both correlation lengths are several times larger than in the case of an uninformative prior distribution. Figure 10 shows the posterior distribution of $\boldsymbol{L_c}$ and the corresponding MAP estimate at its mode. Although the uncertainty in $\boldsymbol{L_c}$ remains large, the informative prior distribution has a strong effect on possible regions of $\boldsymbol{L_c}$, as not much of the probability mass of $f(\boldsymbol{L_c}|\mathbf{M}, \gamma)$ remains in regions of extremely small or large correlation lengths (unlike panel a of Figure 8). The local maxima in the bottom right corner remains unaffected by the informative prior distribution.
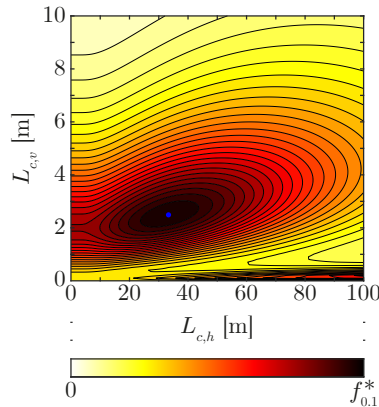

Figure 10: Posterior distribution of the correlation lengths in horizontal ($L_{c,h}$) and vertical ($L_{c,v}$) direction for $\nu = 0.5$ and $\gamma = 0.1$ with informative prior $\mathcal{NG}$ distribution parameters. The blue dot indicates the MAP estimate at the mode of the posterior distribution. $f_{0.1}^*$ is the value of $f(\boldsymbol{L_c}|\mathbf{M}, \gamma)$ at the distribution mode.

The posterior $\mathcal{NG}$ parameters corresponding to the MAP estimate are calculated as

$$[\mu_n, \kappa_n, \alpha_n, \beta_n] = [2.67, \ 6.59, \ 46.52, \ 13.67]. \tag{51}$$

While μ_n is close to the value obtained with the non-informative prior distribution, the other parameters differ. The global characteristic value of the posterior predictive RF $f_c(\boldsymbol{z})$ is $5.5 \, \text{MPa}$, i.e., it is significantly smaller than when using the non-informative prior distribution ($8.2 \, \text{MPa}$). Figure 11 shows the spatial characteristic value $f_{c,\text{k}}(\boldsymbol{z})$ for the $z_1 - z_3$ plane in which the core samples have been taken. The larger correlation lengths lead to an increased area that is affected by the measurement values, in this case spanning almost all over the chamber wall.
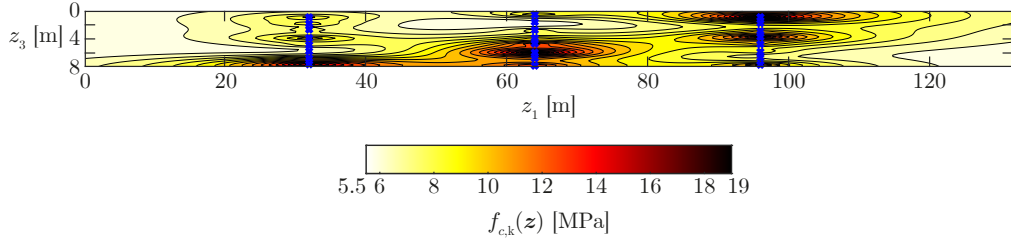
Figure 11: Spatial characteristic value $f_{c,k}(\boldsymbol{z})$ of the posterior predictive random field with informative prior and $\gamma = 0.1$.

3.2. Ship lock Feudenheim

This ship lock is located at the river Hunte in Feudenheim, a district of Mannheim, Germany, and was built in the 1920s. It consists of two chambers and three chamber walls, which are made of unreinforced tamped concrete. The chamber walls have a length of $108\,\mathrm{m}$, a height of $14.5\,\mathrm{m}$ and are separated into six construction blocks of equal length. The amount of data in this study is significantly larger than in the previous study, with a total of 369 measurement values of the concrete compressive strength from 18 vertical core samples (6 core samples per chamber wall, where one core sample has been extracted from each construction block). The three walls are analyzed independently, since there is no knowledge about the construction process available.

As in Section 3.1, a smoothness parameter of $\nu = 0.5$ is employed for the Matérn correlation model. It is assumed that the concrete strength in different construction blocks is not spatially correlated. Hence, the horizontal correlation length cannot be learned because only one vertical core sample is available for each construction block.

As before, a non-informative $\mathcal{NG}$ prior distribution is chosen with parameters given in Equation (40).

3.2.1. Learning the correlation model

To learn the free correlation parameters, namely γ and $L_{c,v}$, the optimization problem of Equation (22) is solved for each wall, resulting in the following MAP estimates:

$$\text{left chamber wall}: \quad \left[L_{c,v}^*,\ \gamma^*\right] = [0.64\,\mathrm{m},\ 0.70], \tag{52}$$

$$\text{middle chamber wall}: \quad \left[L_{c,v}^*,\ \gamma^*\right] = [2.72\,\mathrm{m},\ 0.86], \tag{53}$$

$$\text{right chamber wall}: \quad \left[L_{c,v}^*,\ \gamma^*\right] = [2.32\,\mathrm{m},\ 0.75]. \tag{54}$$

According to the MAP estimates, the RF variability is dominated by the micro-scale variability and the meso-scale variability only plays a minor role. The joint posterior distributions of γ and $L_{c,v}$ are illustrated in Figure 12. In the left chamber wall (panel a), most of the probability mass of $f(L_{c,v}, \gamma | \mathbf{M})$ concentrates in a region of small vertical correlation length, while it distributes over a broad range of γ. The situation

22

is different for the middle and right chamber wall, where the probability mass is concentrated in a region of $\gamma \approx 0.6 - 0.8$, while a broad range of $L_{c,v}$ is covered. It is noted, that the case $\gamma = 1$ is equivalent to a correlation length of $0\,\mathrm{m}$, resulting in a white noise random field without any spatial correlation. This equivalence is the reason for the tail of $f(L_{c,v}, \gamma | \mathbf{M})$ towards small values of $L_{c,v}$ for small values of γ in Figure 12, i.e., the model accounts for the micro-scale variability through $L_{c,v}$ instead of γ in these regions.
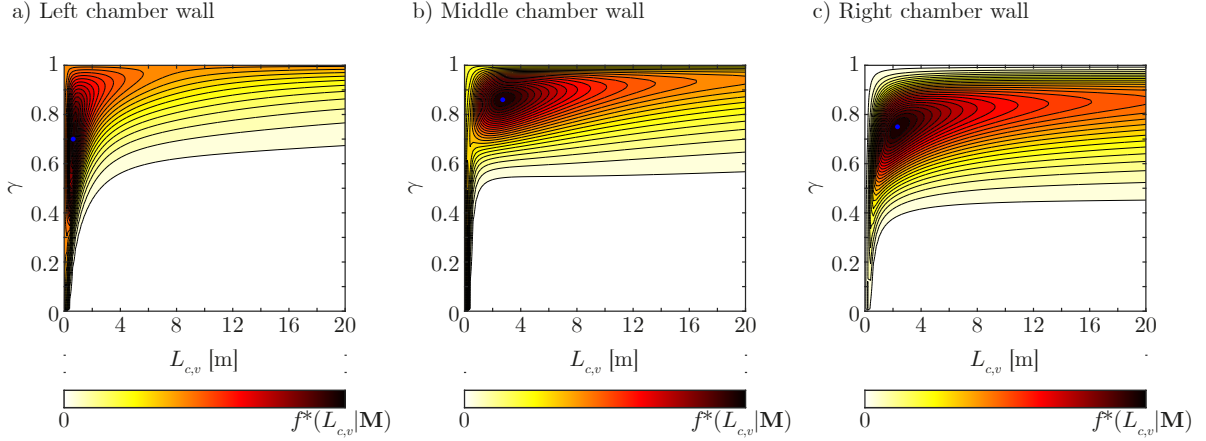

Figure 12: Posterior distribution of the vertical correlation length $L_{c,v}$ and the parameter γ for the left, middle and right chamber wall of the Feudenheim ship lock. The blue dots indicate the MAP estimates at the respective modes of the posterior distribution. $f^*(L_{c,v}, \gamma | \mathbf{M})$ indicates the value of $f(L_{c,v}, \gamma | \mathbf{M})$ at the respective distribution modes.

3.2.2. Spatial posterior predictive concrete compressive strength

A horizontal correlation length needs to be chosen for the Bayesian RF update, since it cannot be learned from the data. The previous results show that the correlation length is a sensitive choice with a strong influence on the posterior predictive RF. For illustration purposes, we choose $L_{c,h} = 5\,\mathrm{m}$, as recommended in [13]. The following posterior parameters for the $\mathcal{NG}$ distribution are calculated:

$$\text{left chamber wall}: \quad [\mu_n, \kappa_n, \alpha_n, \beta_n] = [1.94,\ 72.51,\ 46.5,\ 11.79], \tag{55}$$

$$\text{middle chamber wall}: \quad [\mu_n, \kappa_n, \alpha_n, \beta_n] = [2.17,\ 70.47,\ 73.5,\ 16.06], \tag{56}$$

$$\text{right chamber wall}: \quad [\mu_n, \kappa_n, \alpha_n, \beta_n] = [2.21,\ 48.82,\ 62,\ 19.28]. \tag{57}$$

Each chamber wall is split into 6 spatially independent RFs corresponding to the construction blocks. These are only correlated through the inter-structure variability, i.e., they have the same posterior $\mathcal{NG}$ distribution parameters. The posterior predictive RFs are determined and the resulting $5\%-$quantile values in the $z_1 - z_3$ plane of the measurement locations are illustrated in Figure 13. The left chamber wall (panel a) shows the
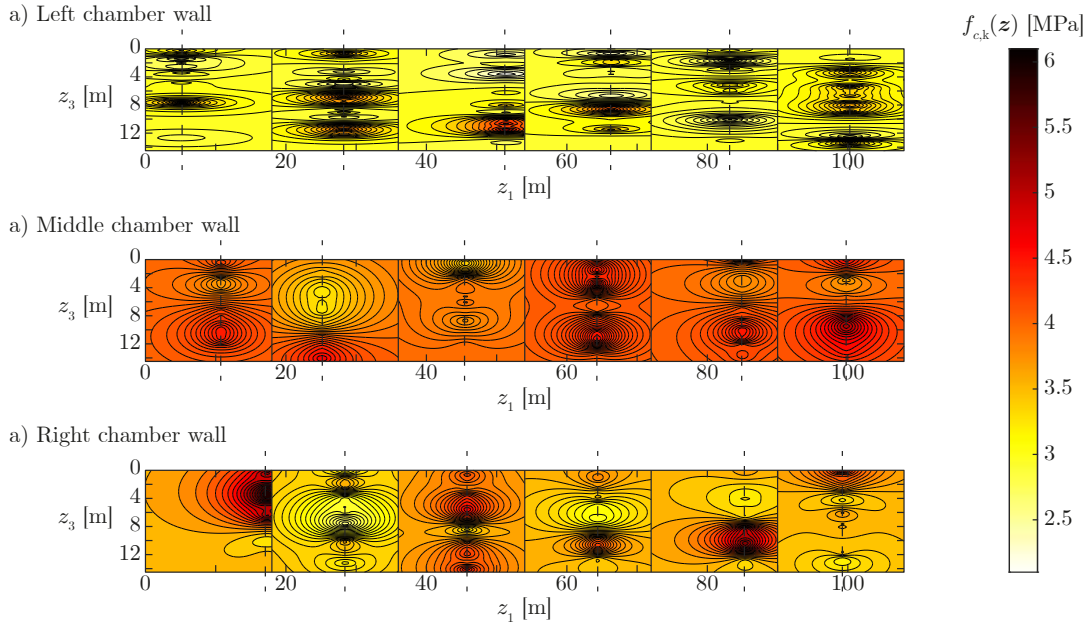
23

Figure 13: Spatial characteristic value $f_{c,k}(\boldsymbol{z})$ of the posterior predictive random fields for the three chamber walls of the ship lock Feudenheim. Each wall is split into six blocks. The locations of the core samples are indicated by the dashed lines.

largest variability in the spatial characteristic value, since it has the smallest vertical correlation lengths. Regions of high (low) characteristic values can be clearly identified and are located close to high (low) measurement values. In the middle chamber wall (panel b), the spatial variability of the characteristic value is small compared to panel a. This is due to the dominance of the micro-scale variability, which reduces the impact of the spatial variability. In addition, the vertical correlation length is significantly larger than in panel a, which leads to a smoother spatial behavior of the RF. The correlation length of the right chamber wall (panel c) is in the same range as the one in panel b, whereas the micro-scale variability is closer to the value of panel a. This leads to larger regions of high (low) characteristic values (in vertical direction) than in panel a and a smooth spatial variability. In general, γ is large in all three chamber walls, which leads to a relatively small range of $f_{c,k}(\boldsymbol{z})$.

3.2.3. Influence of the smoothness parameter

So far, the smoothness parameter of the Matérn correlation model has been set to $\nu = 0.5$. A study on ν is carried out to investigate the effect of that choice. To this end, two additional choices of ν are analyzed, namely $\nu = 2.5$ and $\nu \to \infty$. The following MAP estimates are obtained for the parameters of the

24

correlation model of the left chamber wall:

$$\nu = 2.5 : \quad \left[L_{c,v}^*, \ \gamma^*\right] = [0.66 \, \text{m}, \ 0.75], \tag{58}$$

$$\nu \to \infty : \quad \left[L_{c,v}^*, \ \gamma^*\right] = [0.62 \, \text{m}, \ 0.75], \tag{59}$$

which are relatively close to the MAP estimates for $\nu = 0.5$ ($[L_{c,v}^*, \ \gamma^*] = [0.64 \, \text{m}, \ 0.70]$). The same holds for the posterior $\mathcal{NG}$ distribution parameters, which result in

$$\nu = 2.5 : \quad [\mu_n, \kappa_n, \alpha_n, \beta_n] = [1.94, \ 71.84, \ 46.5, \ 11.79], \tag{60}$$

$$\nu \to \infty : \quad [\mu_n, \kappa_n, \alpha_n, \beta_n] = [1.94, \ 72.31, \ 46.5, \ 11.78], \tag{61}$$

compared to $[\mu_n, \kappa_n, \alpha_n, \beta_n] = [1.94, \ 72.51, \ 46.5, \ 11.79]$ for $\nu = 0.5$. We select a single construction block of the left chamber wall ($z_1 \in [36 \, \text{m}, \ 54 \, \text{m}]$) to perform the spatial update. The resulting $5\%-$quantile values in the $z_1 - z_3$ plane of the measurement locations are illustrated in Figure 14. The smoother correlation model leads to a smoother spatial characteristic value, especially in regions with several measurements close to each other, as can be seen by the increasing smoothness of the contour lines in panel b and c compared to panel a. However, the overall contribution of ν to $f_{c,k}(\boldsymbol{z})$ is minor in this case.
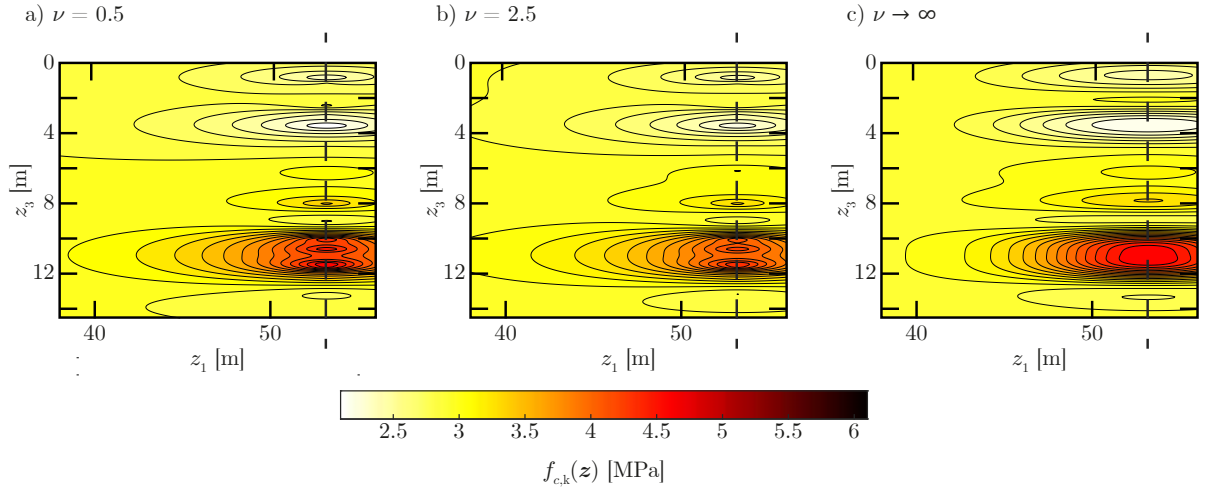

Figure 14: Spatial characteristic value $f_{c,k}(\boldsymbol{z})$ of the posterior predictive random field in a single block of the left chamber wall ($z_1 \in [36 \, \text{m}, \ 54 \, \text{m}]$) for different choices of the smoothness parameter ν. The dashed line indicates the location of the core sample.

3.3. Interpretation of results

The two examples in Sections 3.1 and 3.2 demonstrate the ability of the proposed model to learn the spatial distribution of the concrete strength. The two structures differ in the construction process and the

25

availability of data. The results show that the identification of the parameters of the correlation model is a critical factor of the presented model that significantly impacts the resulting predictions, e.g., the spatial distribution of the characteristic value. Learning the parameters of the proposed correlation model from the data is a challenging task, especially because only limited data is typically available. This is illustrated by the obtained posterior distributions of the correlation parameters, which are rather flat. A prior reduction of the uncertainty in the correlation parameters proves difficult, as the relevant literature is scarce. The anisotropy of the concrete compressive strength RF, confirmed by the data in the first example, results in an additional parameter of the spatial correlation function, adding further to the problem. Significant differences are observed in the estimated correlation parameters, not only for different structures but also for different structural elements, indicating the difficulty in identifying an appropriate correlation function with limited data.

The spatial behavior of the posterior predictive characteristic value, defined as the point-wise $5\%-$quantile value of the resulting log-Student's t-distribution, strongly depends on the micro-scale component of the correlation function. A strong micro-scale variability reduces the spatial correlation and the spatial influence of the measurements. In the latter case, the characteristic value is dominated by the marginal distribution away from the measurements, which is determined by the parameters of the marginal distribution of the RF. If the variability is dominated by a strong micro-scale variability, the choice of the smoothness parameter for the correlation function only plays a minor role.

The unidentifiability of the correlation parameters with limited amount of data can partially be attributed to the equivalence of limiting cases of the parameter values. If the variability is completely defined by the micro-scale variability, the spatial correlation function and its parameters are irrelevant, the resulting RF will have no spatial correlation, i.e., it is given by a white noise field. The same result is obtained when the correlation lengths are zero, in which case the meso-scale correlation function reduces to the Dirac function.

4. Concluding remarks

We propose a new spatial probabilistic model for the concrete strength, which is hierarchical and distinguishes micro-scale and meso-scale variability. Our modeling approach enables the use of spatially distributed measurements of the concrete strength to learn the parameters of its spatial correlation function. The predictive distribution of the proposed random field given the spatial measurements can be obtained in closed form and can be further used in structural verification predictions. The proposed model enables a detailed probabilistic description of the spatial distribution of the concrete strength in existing structures. This allows identification of critical regions within the structure, which can be used for further investigation of the structural condition.

The results show that additional empirical studies are required for effective learning of the correlation

26

function and prior parameters of the concrete compressive strength (prior parameters of the $\mathcal{NG}$ distribution). Particularly, a reliable identification of the anisotropic behavior of the concrete strength in the investigated structures requires additional studies based on horizontal and vertical core samples. Although learning a random field model without spatial information is possible, much of the potential information is lost when the measurement values are not assigned a location. Hence, for effective application of the spatial modeling approach, detailed documentation of the measurement location is inevitable, which is not always the case in practical applications.

The resulting predictive random field model offers opportunities for application in advanced modeling approaches, e.g., in reliability analyses with finite element models accounting for the spatial variability of the concrete material, which is not possible with the standard approaches for learning concrete strength from data. When integrating the random field model in standard structural analysis, spatial averaging of the random field over the areas associated with the relevant failure modes ensures a consistent treatment of the spatial variability [51].

The proposed model can be used also to identify regions within the structure, where additional measurements should be taken, e.g., in the context of inspection planning and maintenance schemes. It can also help to validate potential outliers in the data set by comparing them to measurements close-by and to avoid a selection bias originating from the fact that several measurements are taken from a single core sample.

Appendix A. The log-Student's *t*-distribution

The marginal distribution of the predictive RF for the concrete compressive strength f_c is the log-Student's *t*-distribution. Thus, $f_{c,\ln} = \ln(f_c)$ follows the Student's *t*-distribution with following PDF [52]:

$$f_t(f_{c,\ln}) = \frac{\Gamma\left(\frac{\nu_t}{2} + \frac{1}{2}\right)}{\Gamma\left(\frac{\nu_t}{2}\right)} \left(\frac{\lambda_t}{\pi \nu_t}\right)^{\frac{1}{2}} \left(1 + \frac{\lambda_t \left(f_{c,\ln} - \mu_t\right)^2}{\nu_t}\right)^{-\frac{\nu_t}{2} - \frac{1}{2}}. \tag{A.1}$$

Therein, $\Gamma(\cdot)$ is the gamma function, and μ_t, λ_t and ν_t are the location parameter, scale parameter and degrees of freedom of the Student's *t*-distribution. The PDF of f_c can then be derived as [47, 22]

$$f_{t,\ln}(f_c) = \frac{1}{f_c} f_t\left(\ln(f_c)\right). \tag{A.2}$$

27

The CDF of f_c is defined in terms of the CDF of $f_{c,\ln}$:

$$F_{t,\ln}(f_c) = F_t\left(\ln\left(f_c\right)\right). \tag{A.3}$$

$F_t(\ln\left(f_c\right))$ can be written in closed form in terms of the regularized incomplete beta function. Alternatively, it can easily be evaluated numerically. We note that the log-Student's t-distribution has infinite moments of any order [22].

References

[1] H. Madsen, S. Krenk, N. Lind, Methods of Structural Safety, Dover Civil and Mechanical Engineering, Dover Publications, 2006.

[2] R. Melchers, A. Beck, Structural reliability analysis and prediction, 3rd Edition, John Wiley & Sons, Hoboken, NJ, 2018.

[3] EN 1990:2021-10. Eurocode 0: Basis of structural desgin, European Standard, 2021.

[4] EN 1992-1-1:2011-01. Eurocode 2: Design of concrete structures - Part 1-1: General rules and rules for buildings, European Standard, 2011.

[5] EN 1993-1-1:2010-12. Eurocode 3: design of steel structures - part 1-1: general rules and rules for buildings, European Standard, 2010.

[6] EN 12504-2:2021. Testing concrete in structures - Part 1: Cored specimens - Taking, examining and testing in compression, European Standard, 2021.

[7] EN 13791:2019. Assessment of in-situ compressive strength in structures and precast concrete components, European Standard, 2019.

[8] Bundesanstalt für Wasserbau, BAW-Merkblatt: Bewertung der Tragfähigkeit bestehender, massiver Wasserbauwerke [BAW guideline: Assessment of the bearing capacity of existing, massive hydraulic structures] (2016).

[9] R. Rackwitz, Predictive distribution of strength under control, Matériaux et Constructions 16 (1983) 259 – 267.

[10] L. Fischer, Bestimmung des 5%-Quantils im Zuge der Bauwerksprüfung [Determination of 5% quantile values in the course of inspection of structures], Bautechnik 72 (11) (1995) 712 – 721.

[11] ISO 5725-1:1994. Accuracy (trueness and precision) of measurement methods and results - Part 1: General principles and definitions, International Standard, 1994.

[12] E. Vanmarcke, Random fields: analysis and synthesis, revised and expanded new Edition, World Scientific, 2010.

[13] JCSS probabilistic model code. Part 3 - resistance models, Joint Committee on Structural Safety, 2001.

[14] S. Geyer, I. Papaioannou, C. Kunz, D. Straub, Reliability assessment of large hydraulic structures with spatially distributed measurements, Structure and Infrastructure Engineering 16 (2020) 599 – 612.

[15] J. Chen, J. He, X. Ren, J. Li, Stochastic harmonic function representation of random fields for material properties of structures, Journal of Engineering Mechanics 144 (7) (2018) 04018049.

[16] M. Grigoriu, E. Garboczi, C. Kafali, Spherical harmonic-based random fields for aggregates used in concrete, Powder Technology 166 (3) (2006) 123 – 138.

[17] G. Stefanou, D. Savvas, P. Metsis, Random material property fields of 3D concrete microstructures based on CT image reconstruction, Materials 14 (6) (2021) 1423.

[18] A. Masi, A. Digrisolo, G. Santarsiero, Analysis of a large database of concrete core tests with emphasis on within-structure variability, Materials 12 (12) (2019) 1985.

[19] J. Tao, J. Chen, A hierarchy model for the uncertainty quantification of spatial variability in the constitutive parameters of concrete in structures, Structural Safety 95 (2022) 102181.

[20] S. Geyer, I. Papaioannou, D. Straub, Characteristic values of spatially varying material properties in existing structures, in: A. Chen, X. Ruan, D. M. Frangopol (Eds.), Proceedings of the seventh international symposium on life-cycle civil engineering, CRC Press/Balkema, 2020, pp. 479 − 486.

[21] A. Gelman, J. Carlin, H. Stern, D. Dunson, A. Vehtari, D. Rubin, Bayesian data analysis, 3rd Edition, Chapman & Hall/CRC texts in statistical science, CRC, Boca Raton, FL, 2013.

[22] S. Geyer, I. Papaioannou, D. Straub, Bayesian analysis of hierarchical random fields for material modeling, Probabilistic Engineering Mechanics 66 (2021) 103167.

[23] A. M. Freudenthal, Safety and the probability of structural failure, Transactions of the American Society of Civil Engineers 121 (1) (1956) 1337 − 1375.

[24] J. Benjamin, C. Cornell, Probability, Statistics, and Decision for Civil Engineers, new Edition, Dover Books on Engineering, Dover Publications, 2014.

[25] EN 206-1:2000. Concrete - Part 1: Specification, performance, production and conformity, European Standard, 2000.

[26] A. Neville, Properties of Concrete, 5th Edition, Pearson, 2011.

[27] Z. P. Bažant, Size effect on structural strength: a review, Archive of Applied Mechanics 69 (9) (1999) 703 − 725.

[28] M. Kersken-Bradley, R. Rackwitz, Stochastic Modeling of Material Properties and Quality Control, JCSS working document, International Association for Bridge and Structural Engineering, 1991.

[29] P. Abrahamsen, A review of Gaussian random fields and correlation functions, 2nd Edition, Norwegian Computing Center, 1997.

[30] B. Sudret, A. Der Kiureghian, Stochastic finite element methods and reliability. A state-of-the-art report, Report on research No. UCB/SEMM-2000/08, University of California, Berkeley (2000).

[31] Y. Liu, J. Li, S. Sun, B. Yu, Advances in Gaussian random field generation: a review, Computational Geosciences 23 (5) (2019) 1011 − 1047.

[32] M. Grigoriu, Crossings of non-Gaussian translation processes, Journal of Engineering Mechanics 110 (4) (1984) 610 − 620.

[33] C. Li, A. D. Kiureghian, Optimal discretization of random fields, Journal of Engineering Mechanics 119 (6) (1993) 1136 − 1154.

[34] H. Rüsch, R. Sell, R. Rackwitz, Statistische Analyse der Betonfestigkeit [Statistical analysis of concrete strength], Deutscher Ausschuss für Stahlbeton 206, 1969.

[35] R. J. Torrent, The log-normal distribution: a better fitness for the results of mechanical testing of materials, Matériaux et Construction 11 (4) (1978) 235 − 245.

[36] B. Matérn, Spatial variation, 2nd Edition, Lecture notes in statistics, Springer, New York City, NY, 1986.

[37] H. Zhu, L. Zhang, Characterizing geotechnical anisotropic spatial variations using random field theory, Canadian Geotechnical Journal 50 (7) (2013) 723 − 734.

[38] EN 12504-2:2019. Testing concrete in structures - Part 2: Non-destructive testing - Determination of rebound number, European Standard, 2019.

[39] EN 12504-4:2019. Testing concrete in structures - Part 4: Determination of ultrasonic pulse velocity, European Standard, 2019.

[40] A. Westendarp, H. Becker, J. Bödefeld, H. Fleischer, C. Kunz, M. Maisner, H. Müller, A. Rahimi, T. Reschke, F. Spörel, Erhaltung und Instandsetzung von massiven Verkehrswasserbauwerken [Maintenance and repair of massive hydraulic structures], Beton-Kalender 2015, John Wiley & Sons, 2015, Ch. IV, pp. 185 − 246.

[41] EN 12390-6:2009. Testing hardened concrete - Part 6: Tensile splitting strength of test specimens, European Standard, 2009.

[42] K.-K. Phoon, F. H. Kulhawy, Characterization of geotechnical variability, Canadian Geotechnical Journal 36 (4) (1999) 612 − 624.

[43] F. E. Grubbs, Sample criteria for testing outlying observations, The Annals of Mathematical Statistics 21 (1) (1950) 27 – 58.

[44] W. J. Dixon, Analysis of extreme values, The Annals of Mathematical Statistics 21 (4) (1950) 488 – 506.

[45] S. Brooks, A. Gelman, G. Jones, X.-L. Meng, Handbook of Markov chain Monte Carlo, Chapman & Hall/CRC handbooks of modern statistical methods, CRC, Boca Raton, FL, 2011.

[46] M. DeGroot, Optimal Statistical Decisions, McGraw-Hill series in probability and statistics, McGraw-Hill, New York City, NY, 1969.

[47] L. H. Vanegas, G. A. Paula, Log-symmetric distributions: statistical properties and parameter estimation, Brazilian Journal of Probability and Statistics 30 (2) (2016) 196 – 220.

[48] K. P. Murphy, Machine learning: a probabilistic perspective, Adaptive computation and machine learning, MIT, Cambridge, MA, 2013.

[49] C. P. Robert, The Bayesian choice: from decision-theoretic foundations to computational implementation, 2nd Edition, Springer texts in statistics, Springer, 2007.

[50] S. Pöhlmann, R. Rackwitz, Zwei Schätzprobleme bei Gauß'schen Folgen [Two estimation problems with Gaussian sequences], Berichte zur Zuverlässigkeitstheorie der Bauwerke, Sonderforschungsbereich 96, Heft 53, Technische Universität München (1981).

[51] S. Geyer, I. Papaioannou, L. Graham-Brady, D. Straub, The spatial averaging method for non-homogeneous random fields with application to reliability analysis, Engineering Structures 253 (2022) 113761.

[52] C. M. Bishop, Pattern recognition and machine learning, Information science and statistics, Springer, New York City, NY, 2006.